Biosensors and Bioelectronics 42 (2013) 496–502

Contents lists available at SciVerse ScienceDirect

Biosensors and Bioelectronics

journal homepage: www.elsevier.com/locate/bios

Microfluidic characterization of specific membrane capacitance and cytoplasm conductivity of single cells

Yi Zheng [a,b], Ehsan Shojaei-Baghini [a], Chen Wang [d,e,*], Yu Sun [a,b,c,**]

[a] Department of Mechanical and Industrial Engineering, University of Toronto, Toronto, ON, Canada
[b] Institute of Biomaterials and Biomedical Engineering, University of Toronto, Toronto, ON, Canada
[c] Department of Electrical and Computer Engineering, University of Toronto, Toronto, ON, Canada
[d] Department of Pathology and Laboratory Medicine, Mount Sinai Hospital, Toronto, ON, Canada
[e] Department of Laboratory Medicine and Pathobiology, University of Toronto, Toronto, ON, Canada

ARTICLE INFO

Article history:
Received 23 September 2012
Received in revised form
23 October 2012
Accepted 24 October 2012
Available online 2 November 2012

Keywords:
High-throughput
Impedance spectroscopy
Microfluidics
Electrical characterization
Single cells
Cell classification

ABSTRACT

This paper presents a technique for single-cell electrical property (specific membrane capacitance and cytoplasm conductivity) characterization at a speed of 5–10 cells/s (vs. minutes/cell using existing techniques such as patch clamping and electrorotation). When a cell flows through a microfluidic constriction channel which is marginally smaller than the diameter of tested cells, electrical impedance at multiple frequencies is measured. Electrical and geometrical models are developed to interpret the impedance data and to determine the specific membrane capacitance and cytoplasm conductivity of individual cells. Results from testing 3249 AML-2 cells and 3398 HL-60 cells reveal different specific membrane capacitance and cytoplasm conductivity values between AML-2 (12.0 ± 1.44 mF/m^2, 0.62 ± 0.10 S/m) and HL-60 (14.5 ± 1.75 mF/m^2, 0.76 ± 0.12 S/m) cells. The results also demonstrate that the quantification of specific membrane capacitance and cytoplasm conductivity can enhance cell classification results since these parameters contain information additional to cell size.

1. Introduction

Each cell type has unique membrane contents and intracellular structures to fulfill their specific physiological functions. The membrane and intracellular compositions determine the cell's electrical properties that can reflect cell physiological states and can possibly serve as label-free markers for cell type classification. Compared to conventional biochemical techniques (e.g., flow cytometry), which rely on the labeling of targeted cells with fluorescence-conjugated antibodies or molecules to distinguish between cell types, electrical measurement has distinct simplicity in sample preparation (no labeling), and in data recording and processing (Sun and Morgan, 2010; Valero et al., 2010; Zheng et al., 2012).

In order to interpret the electrical properties of a cell, a single shell model is widely used in various measurement setups (Schwan 1957, 1968). The cell is modeled as a dielectric thin membrane enclosing homogenous spherical cytoplasm. Accordingly, the specific membrane capacitance, which is affected by the membrane morphology, lipid bilayer composition and thickness, and embedded proteins (Wang et al.,1994; Yang et al., 1999; Zimmermann et al., 2008); and cytoplasm conductivity, which is influenced by the nucleus to cytoplasm ratio and the ion concentration inside the cell (Duncan et al., 2008; Holzel, 1999; Huang et al., 1995), are depicted as the inherent electrical properties of the cell's membrane and cytoplasm, respectively. In the past decades, a number of techniques were developed for single-cell electrical measurements. However, existing technologies are either incapable of characterizing the inherent electrical properties or incapable of providing statistically significant data due to limited measurement speed.

The most successful technique performing electrical measurement on single cells is the Coulter counter, where direct current (DC) impedance measurements are made for counting and sizing single cells (Hoffman and Britt, 1979). Impedance flow cytometry is an extension of the Coulter counter technique. It implements both DC and RF impedance measurements. The ratio of the RF signal to DC signal is defined as *opacity*, which is applied in commercial hematology analyzers for three differential counts of white blood cells (Rodriguez et al., 2001; Sequeira and Goltman, 2001). However, the opacity value reflects combined effects from both cell membrane and cytoplasm. It is not an inherent electrical

* Corresponding author at: Department of Pathology and Laboratory Medicine, Mount Sinai Hospital, Toronto, ON, Canada. Tel.: +1 416 586 4469.
** Corresponding author at: Department of Mechanical and Industrial Engineering, University of Toronto, Toronto, ON, Canada. Tel.: +1 416 946 0549; fax: +1 416 978 7753.
E-mail addresses: cwang@mtsinai.on.ca (C. Wang), sun@mie.utoronto.ca (Y. Sun).

0956-5663/$ - see front matter © 2012 Elsevier B.V. All rights reserved.
http://dx.doi.org/10.1016/j.bios.2012.10.081

signature of cells and can differ among different testing configurations (e.g., co-planar electrodes vs. parallel facing electrodes; Sun and Morgan, 2010; van Berkel et al., 2011). μ-EIS (Micro Electrical Impedance Spectroscopy) is a technique in which a frequency-dependent excitation signal is applied across a trapped cell to measure the corresponding current response (Cho and Thielecke, 2007; Han et al., 2006; Li and Lin, 2007). Similar to opacity, capacitance and resistance of a cell are not inherent electrical parameters (vs. specific membrane capacitance and cytoplasm conductivity) and are strongly affected by electrode size, cell trapping mechanism, and cell volume.

The patch-clamp technique was originally developed for measuring current through ion channels on the cell membrane, and can be used for characterizing the specific membrane capacitance by aspirating a cell membrane patch into a micropipette (Schwake et al., 2002; Zhao et al., 2008). However, it is a highly delicate procedure and has strong operator skill dependence. Consequently, the testing speed of patch-clamp is typically tens of minutes per cell, and at most tens of cells can be tested in a study. Electrorotation is capable of quantifying electrical properties of single cells by measuring the rotation rate of cells induced by a rotating electrical field. (e.g., specific membrane capacitance, cytoplasm conductivity and cytoplasm permittivity). Nonetheless, electrorotation is also a rather tedious and slow technique, and it typically takes approximately 30 min to test a single cell (Cristofanilli et al., 2002; De Gasperis et al., 1998). Another drawback is the difficulty to achieve efficient rotation in high conductivity physiological buffer. Hence, electrical properties of the tested cells may have already been altered when immersed in the low conductivity sucrose buffer. At present, no techniques exist for measuring the specific membrane capacitance and cytoplasm conductivity values at a reasonable speed.

This paper presents a new technique for measuring single-cell specific membrane capacitance and cytoplasm conductivity at a speed of 5–10 cells/s. A microfluidic constriction channel that is marginally smaller than the diameters of tested cells concentrates the electrical current to penetrate the cell membrane and confines the geometry of individual cells. Electrical impedance was measured at seven frequencies simultaneously. By fitting experimental impedance measurement data to equivalent circuit models, the specific membrane capacitance and cytoplasm conductivity values of over 6000 cells were quantified. AML-2 and HL-60 cells were selected for their comparable sizes to assess the effectiveness of distinguishing these size-comparable cell types using their electrical parameters. Compared to the impedance measurement system we previously reported (Chen et al., 2011b), the new multi-frequency measurement technique and the improved equivalent circuit model with cell geometry estimation enable, for the first time, the determination of the specific membrane capacitance and cytoplasm conductivity values on a high number of cells (3249 AML-2 cells and 3398 HL-60 cells).

2. System overview

Fig. 1(a) shows the schematic diagram of the single cell electrical measurement system. The microfluidic chip was constructed by bonding PDMS microchannels to a glass slide. Cell suspension was pipetted into the inlet reservoir of the device and driven through the constriction channel by hydraulic pressure difference (500 Pa). Two Ag/AgCl non-polarizable electrodes are plugged into the inlet and outlet ports. A sinusoidal excitation voltage with 7 frequency components (1 kHz, 20 kHz, 50 kHz, 100 kHz, 200 kHz, 300 kHz, 400 kHz, @0.2 V_{pp}) is generated by the function generator. As cells are aspirated through the constriction

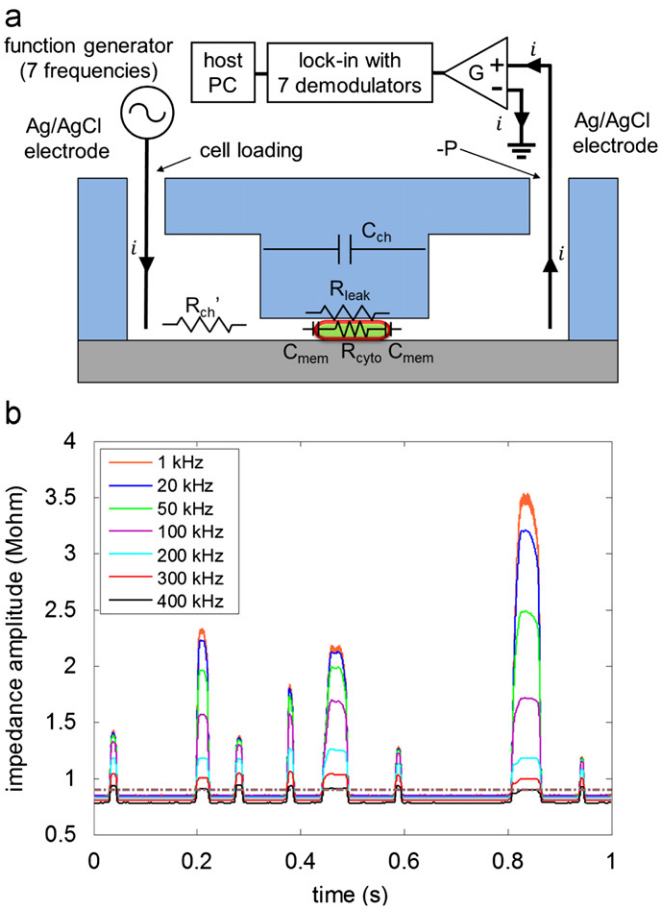

Fig. 1. (a) Schematic of the microfluidic system for electrical measurement of single cells. "-P" denotes the negative pressure used to aspirate cells through the constriction channel. Within the constriction channel, "green" represents the cytoplasm and "red" represents the membrane. "*i*" is the current through the channel. R_{cyto} represents cytoplasm resistance and C_{mem} represents membrane capacitance (on each side of the elongated cell); R_{leak} represents the leaking resistance between cell membrane and channel walls; R_{ch}' and C_{ch} represent resistance of the medium and parasitic capacitance of the channel. (b) Experimental data showing impedance amplitude profiles (at 7 frequencies) measured within 1 s with 8 cells passing through the constriction channel. Impedance profiles of different frequencies are plotted in different colors. (For interpretation of the references to color in this figure legend, the reader is referred to the web version of this article.)

channel continuously, current within the channel is pre-amplified, demodulated and sampled at 14.4 kHz per frequency. By fitting the impedance spectroscopy (7 frequencies) to the equivalent circuit models, membrane capacitance (C_{mem}) and cytoplasm resistance (R_{cyto}) can be obtained. Within the constriction channel, the cells' shape is well confined; hence, the C_{mem} and R_{cyto} values can be used to determine the cell's specific membrane capacitance and cytoplasm conductivity.

Fig. 1(b) shows impedance amplitude profiles (7 frequencies) measured within 1 s with 8 cells passing through the constriction channel. The excitation voltage of a single frequency is 0.2 V_{pp}, which is intentionally selected to provide a measurable current signal and avoid possible electroporation (electroporation threshold voltage is ~0.5 V (Geng et al., 2011; Wang and Lu, 2006)). A threshold is defined in this study to be 1.05 × basal amplitude (i.e., the amplitude without cell presence in the constriction channel) at 1 kHz (see dash–dotted line in Fig. 1(b)). Comparing a signal amplitude value with the threshold, the portions where the impedance amplitude is higher than the threshold value are considered as cell passage regions. The maximal values of each frequency within the cell passing region are extracted and used to

calculate the electrical parameters of the cell. The peak width shown in Fig. 1(b) is the time required for a cell to pass through the constriction channel. It is defined as transit time and determined by cell size and deformability. Transit time is used as a mechanical property indicator of the cell, and detailed discussion on this parameter has been given in the literature (Rosenbluth et al., 2008; Zheng et al., 2012).

3. Materials and methods

Details on device fabrication, cell culture, and experimental protocol are given in the supplementary materials. AML-2 (acute myeloid leukemia) and HL-60 (human promyelocytic leukemia) cells were chosen for testing in this study. Their comparable sizes permit the evaluation of using their electrical parameters (i.e., specific membrane capacitance and cytoplasm conductivity) for cell classification. Furthermore, the characterization of electrical properties of white blood cells (WBCs) has been reported (e.g., using the electrorotation technique), providing reference data for comparison with our measurements. The cross-sectional area of the constriction channel is 9 μm × 9 μm, which was chosen to ensure that all the tested cells can pass through the testing area smoothly and the cell geometry is well confined. WBCs behave like a droplet of viscous liquid and are highly deformable (Bathe et al., 2002; Yap and Kamm, 2007); therefore, they can easily pass through the constriction channel. The size of the channel was designed to be slightly smaller than the cells' diameters. The channel was lubricated by incubating with 1% BSA before use to minimize the friction between cell membrane and channel walls, and to reduce the effect of deformation on cell membrane morphology and biological activity. In experiments, we observed that the cells readily recovered to their original shapes and morphologies after they exited the constriction channel. When a WBC is inside the constriction channel, its geometry is well confined by the channel (Fig. 2(a)). To quantify the geometry of the tested cells, a simplified geometrical model is adopted

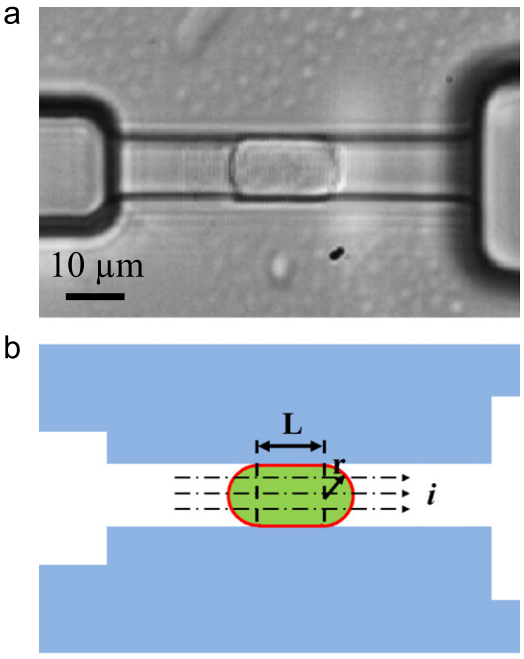

Fig. 2. (a) An AML-2 cell is inside the constriction channel. (b) Schematic representation of the simplified geometrical model ("green" and "red" represent cytoplasm and membrane, respectively). (For interpretation of the references to color in this figure legend, the reader is referred to the web version of this article.)

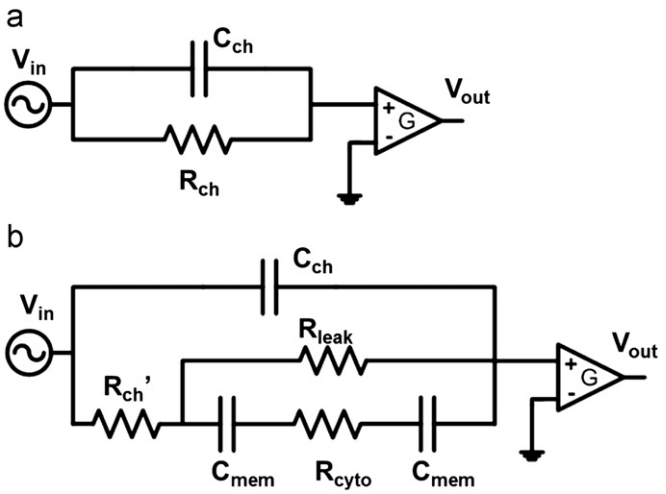

Fig. 3. (a) The channel without cells passing is modeled as a resistor R_{ch} and a capacitor C_{ch} in parallel. (b) The cell is modeled as a resistor R_{cyto} (cytoplasm) and two capacitors C_{mem} (membrane) in series; R_{leak} represents the leaking resistance between cell membrane and channel walls; R_{ch}' represents the medium's resistance after a portion of the constriction channel is occupied by a cell. G is a pre-amplifier converting current into voltage signals.

(Gifford et al., 2003). The cell is modeled as a rectangular cube with two quasi-spherical caps fitted smoothly onto the rectangle (Fig. 2(b)). The caps of the cell are taken as a quasi-sphere, with an effective radius (r) of 1/2 the side of the constriction channel's cross-sectional area (4.5 μm in this case). Under this simplification, the effective area of the membrane (red thin shell around the cells contour) that contributes to the cell's capacitance (C_{mem}) includes only the two quasi-spherical caps' area (determined by the cross-sectional area of the constriction channel); and the elongation L (see Fig. 2(b)) is the only geometrical parameter that varies across different cells, which is only determined by the cells' volume, assuming Poisson's ratio is approximately 0.5 (Hochmuth, 2000).

Fig. 3(a) and (b) show the equivalent circuit models of the system without and with cells in the constriction area. The electrical models are modified from the equivalent models used in patch-clamp (Li and Lin, 2007) and prove effective for interpreting our experimental setup (Chen et al., 2011a). The impedance amplitude $|Z|$ of the system at a specific frequency can be calculated as

$$|Z| = \frac{V_{in}}{V_{out}} G \tag{1}$$

where V_{in} is the amplitude of the excitation voltage (0.2 V in this case), V_{out} is the output of the pre-amplifier, and G (10,000 Ω in this case) is the gain of the pre-amplifier.

When there is no cell present in the constriction region, the channel is equivalent to a resistor R_{ch} and a capacitor C_{ch} connected in parallel. R_{ch} is the resistance of the medium in between the electrodes determined by the conductivity of the medium and geometries of the channel. C_{ch} is the parasitic capacitance of the channel. R_{ch} and C_{ch} can be obtained by fitting the impedance amplitude profiles to Model 1, before aspiration pressure is applied.

As a cell is present inside the constriction channel, it has an elongation length, L and has membrane capacitance, C_{mem} and cytoplasm resistance, R_{cyto}. The cell blocks the current within the channel causing the impedance to increase. When a portion of the constriction channel is occupied by a cell, R_{ch} is also changed due to the change of the medium volume. The resistance of the medium in the channel with the presence of a cell (R_{ch}') can be

calculated as

$$R_{ch}{}' = R_{ch} - \frac{1}{\sigma}\frac{L}{4r^2} \quad (2)$$

where R_{ch} is the resistance of the channel without the presence of cells, $R_{ch}{}'$ is the resistance of the channel occupied by a cell with elongation L, r is the radius of the quasi-spherical caps (4.5 μm in this case), σ is the conductivity of the medium (1.6 S/m).

At low frequencies, all the capacitive components can be perceived as an open circuit. Thus, the measured low frequency impedance, R_{low}, only reflects R_{leak} and $R_{ch}{}'$ (Eq. (3)). R_{leak} can be calculated as

$$R_{leak} = R_{low} - R_{ch}{}' \quad (3)$$

In Model 2, C_{ch} remains unchanged with or without the presence of cells in the constriction channel. Thus, only the electrical components related to the tested cell remain unknown (R_{cyto} and C_{mem}), which can be obtained by fitting the impedance spectroscopy data to Model 2. Under the geometrical assumption, the specific membrane capacitance and cytoplasm conductivity can be estimated according to

$$\text{Specific membrane capacitance} = \frac{C_{mem}}{2\pi r^2} \quad (4)$$

$$\text{Cytoplasm conductivity} = \frac{L+2r}{4r^2} \times \frac{1}{R_{cyto}} \quad (5)$$

where R_{cyto} and C_{mem} are the resistance and capacitance of the tested cell obtained from curve fitting, respectively, L is cell elongation, and r is the radius of the quasi-spherical caps (4.5 μm in this case). The quasi-spherical caps' surface area is used as the effective area for specific membrane capacitance, and the cross-sectional area of the channel is used as the effective area for cytoplasm conductivity calculation. The cross-sectional area determines the leakage resistance (R_{leak}), cell elongation and effective membrane area. Since our electrical models take these parameters' effect into account, the quantified inherent electrical parameters (specific membrane capacitance and cytoplasm conductivity) are not affected by the constriction area as long as the cell's geometry is well confined.

4. Results and discussion

4.1. Curve fitting and frequency selection

Cells of various diameters were first "parked" in the constriction channel with careful application of very low aspiration pressure. This allows an impedance spectroscopy (201 frequency points within the range 1 kHz–1 MHz) of the parked cells to be attained. In the meanwhile, images of the tested cells were taken via microscopy imaging (Olympus IX81, Olympus Canada Inc., Canada), and cell elongation was measured with a custom-designed image processing program. Fig. 4 shows the impedance amplitude (a) and phase (b) spectroscopy of the constriction channel without and with cells having different diameters. Non-linear least squares curve fitting (MATLAB, Mathworks, USA) was used to fit the measured impedance to the equivalent circuit models. Before a cell was parked, the impedance profile was measured and fitted to Model 1(see Fig. 4(a)) to determine R_{ch} (0.85 Mohm) and C_{ch} (0.18 pF). When a cell was parked in the channel, the impedance spectroscopy was measured and fitted to Model 2 to determined C_{mem} and R_{cyto}. We tested 20 AML-2 cells with 201 frequency points spectroscopy, and the C_{mem} and R_{cyto} were determined to be 1.838 ± 0.240 pF and 0.300 ± 0.057 Mohm, respectively, with all fitting regression coefficients higher than 0.99.

Generally, more frequency points are preferred for impedance spectroscopy to obtain more comprehensive information of the tested system. However, due to the limit of instruments

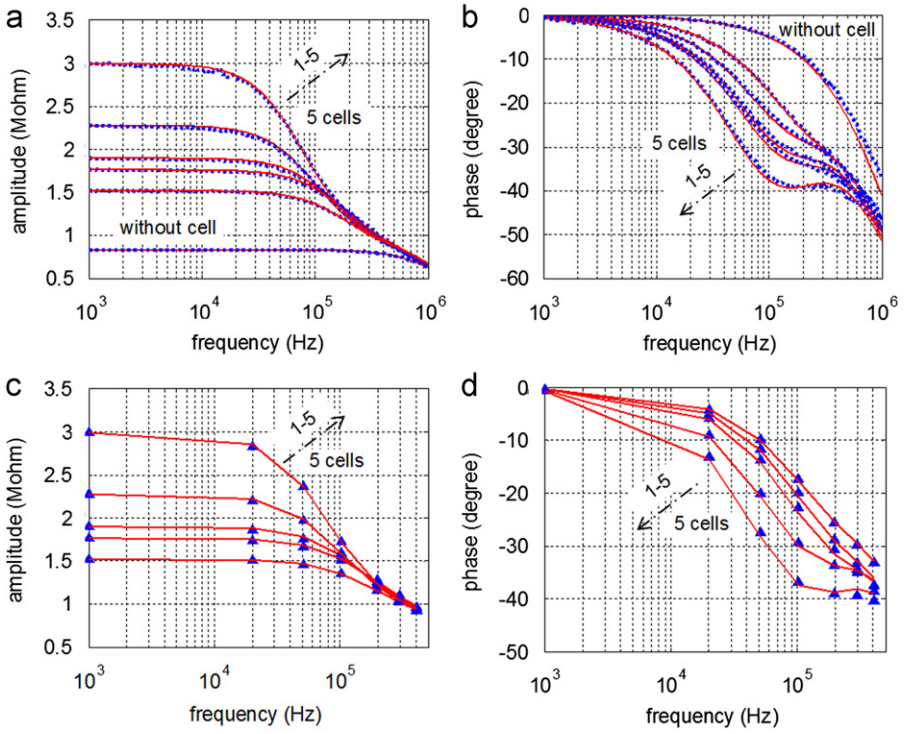

Fig. 4. (a) and (b) Impedance amplitude and phase of the constriction channel without and with cells (5 cells of different diameters), measured at 201 frequency points within the range of 1 kHz–1 MHz. (c) and (d) Impedance amplitude and phase measured at 7 selected frequency points (1 kHz, 20 kHz, 50 kHz, 100 kHz, 200 kHz, 300 kHz, 400 kHz), on the same 5 cells as shown in (a) and (b). Experimental data and curve fitting results are plotted in blue and red, respectively. (For interpretation of the references to color in this figure legend, the reader is referred to the web version of this article.)

(e.g., HF2IS, Zurich Instrument, Switzerland), measurements can only be made at 7 frequencies. Thus, the 7 frequency points must be properly selected. As shown in Fig. 4(a) and (b), the system is almost purely resistive at low frequencies (near 1 kHz–10 kHz), wherein the cell membrane acts as an efficient insulator. This can be seen in the impedance phase of the system (close to 0°). In the range of 1–10 kHz, the impedance amplitude value does not vary much. Hence, the impedance amplitude at 1 kHz is selected to reflect the resistive characteristic of the system. High frequency (near 1 MHz) results in low impedance of C_{ch}, and electrical field lines undesirably obviate the cell in the constriction channel. As a result, the impedance amplitude of the channel with a cell and without a cell becomes rather close, which can barely reflect the cell's electrical properties. Therefore, more frequency points (20 kHz, 50 kHz, 100 kHz, 200 kHz, 300 kHz, 400 kHz) are selected within the middle frequency range for well capturing the cell's electrical properties. The impedance amplitude at the selected 7 frequency points of the same 20 cells was fitted to Model 2 (see Fig. 4(c) and (d)). The calculated C_{mem} and R_{cyto} are 1.836 ± 0.218 pF and 0.316 ± 0.051 Mohm, respectively, which are fairly close to the values obtained from 201 frequency points fitting (1.838 ± 0.240 pF and 0.300 ± 0.057 Mohm). These results prove the validity of the selected 7 frequencies.

4.2. Cell elongation measurement using impedance signal

Cell elongation can be measured using high-speed microscopy imaging. However, high-speed cameras (tens of kHz) generate gigabyte data per second and can only record for a few seconds due to limited memory. Processing this massive amount of image data takes tremendous computation efforts and time. Hence, high-speed imaging for measuring cell elongation (L) is not a desirable approach. Since the cell membrane acts as an insulate layer at low frequencies (lower than 1 kHz), the impedance increase at 1 kHz is only determined by R_{leak}, which is proportional to cell elongation (L). Before high-speed measurements, we correlated the elongation of cells to the impedance increase (ΔR) at 1 kHz by microscopy imaging and manually measuring tens of cells' elongation in the captured images (see Fig. 5). The fitted relationship was then used to estimate cell elongation in the subsequent all-electrical high-throughput experiments. Compared with HL-60, AML-2 is less deformable (Lam et al., 2007), leading to a slightly larger gap between AML-2 cell membrane and the corners of the rectangle-like microchannels. Thus, as shown in Fig. 5, with the same elongation, AML-2 cells caused a lower impedance increase compared to HL-60 cells, resulting in the different slopes of linear trends between AML-2 and HL-60 cells.

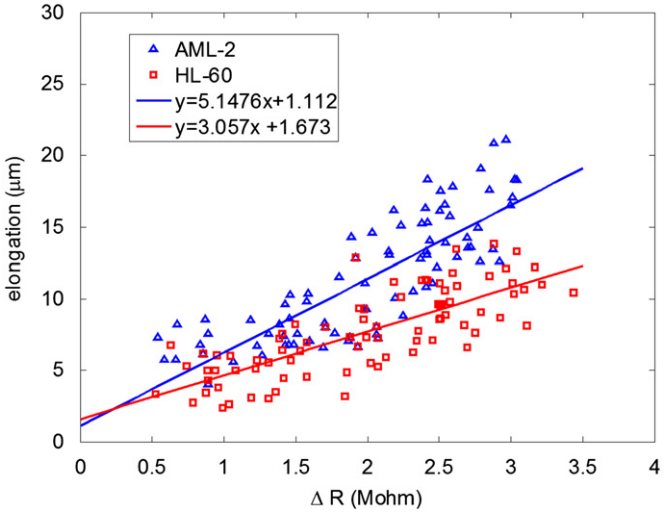

Fig. 5. Experimental correlation between cell elongation and impedance increase at 1 kHz of AML-2 (blue) and HL-60 (red). (For interpretation of the references to color in this figure legend, the reader is referred to the web version of this article.)

4.3. Specific membrane capacitance and cytoplasm conductivity

Our microfluidic system tested AML-2 cells and HL-60 cells. Impedance profiles were recorded and fed into an automated curve fitting program. The program outputs values of specific membrane capacitance, cytoplasm conductivity, cell elongation and norm of the curve fitting. Although intact cells represent the majority in the tested cell suspension, there were also debris, clusters, and apoptotic cells. All the data points shown in Fig. 5 were measured on intact single cells as verified in experiments via imaging. The data revealed that impedance increase at 1 kHz (ΔR) falls into the range of 0.3–3.5 Mohm for the intact single cell events. Thus, the events with impedance increase at 1 kHz (ΔR) out of this range were regarded as debris or clusters and were excluded from the final data. In the meanwhile, since the C_{mem} values of the apoptotic cells are so low that the curve fitting program is not able to locate a solution within the reasonable range, the events with exceptionally high curve fitting norm are regarded as apoptotic cells (confirmed via imaging) and excluded from the final results (see Fig. S2). Using these criteria, approximately 5% of events were excluded. Fig. 6(a) shows the scatter plot of specific membrane capacitance vs. cytoplasm conductivity of AML-2 ($n=3249$) and HL-60 ($n=3398$). Both parameters were quantified and fitted to normal distributions (see Fig. 6(b)). The determined specific membrane capacitance and cytoplasm conductivity of AML-2 and HL-60 are 12.0 ± 1.44 mF/m^2, 0.62 ± 0.10 S/m and 14.5 ± 1.75 mF/m^2, 0.76 ± 0.12 S/m, respectively. The difference in specific membrane capacitance values can be attributed to the differences in the two cell types' surface morphology (Gamliel et al., 1983). Membrane morphology was confirmed to be a primary factor influencing cells' specific membrane capacitance (Wang et al., 1994; Yang et al., 1999). Additionally, the different nucleus-to-cytoplasm ratios of these two cell types, as we observed in imaging, could have contributed to the measured differences in cytoplasm conductivity.

4.4. Error analysis

Cell elongation is estimated by using the correlation of cell elongation and the impedance increase at 1 kHz (Fig. 5). The error can be quantified to be

$$\Delta L = \frac{1}{N}\sum_{i}^{N} |y_i - f_i| \tag{6}$$

where ΔL is the average error of cell elongation measurement, y_i is cell elongation measured via microscopy imaging, f_i is the predicted value calculated via the fitted relationships, and N is the total number of data points. According to Eq. (6), the average elongation measurement errors of AML-2 and HL-60 are 2.03 μm and 1.48 μm, respectively. When the cell elongation is used for the estimation of R_{ch}' (Eq. (2)), the error in elongation estimate can cause an error of 0.01–0.03 Mohm of R_{ch}', which accounts for less than 3.5% of R_{ch}'. Furthermore, R_{ch}' is much smaller compared with the impedance value of R_{cyto} and C_{mem}. Thus, the elongation errors' effect on the electrical component calculation (R_{cyto} and C_{mem}) is negligible. However, the elongation error can lead to 7–12% errors in cytoplasm conductivity estimation (Eq. (5)).

We further investigated the effect of cell size on the measured specific membrane capacitance and cytoplasm conductivity of

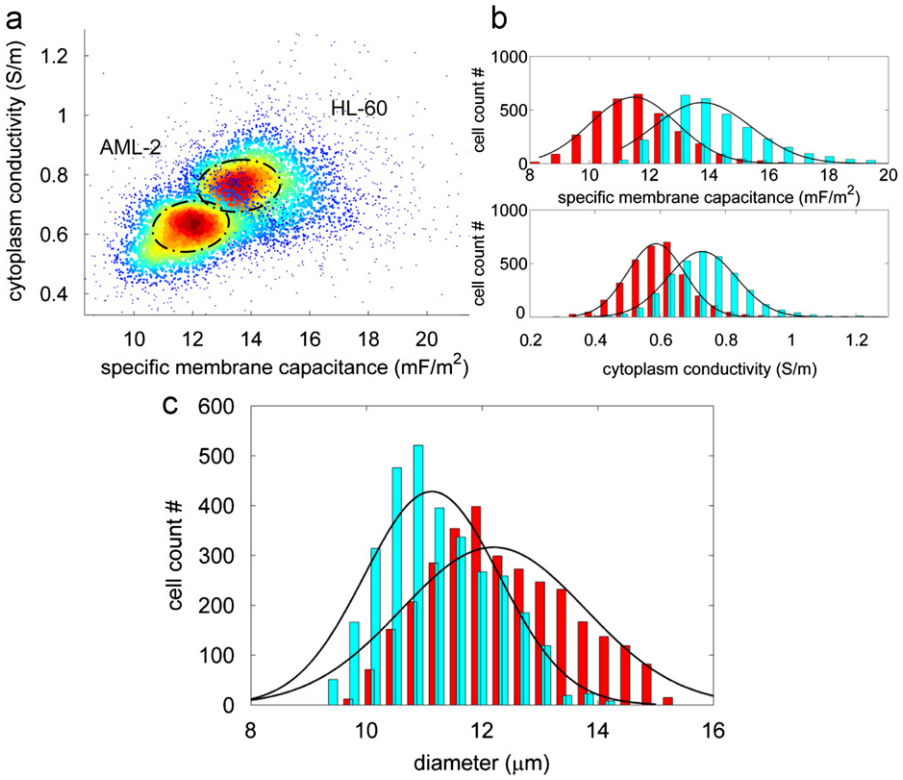

Fig. 6. (a) Scatter plot of specific membrane capacitance vs. cytoplasm conductivity of AML-2 and HL-60. Color coding represents data distribution densities (High■→Low■). (b) Histograms of specific membrane capacitance and cytoplasm conductivity of AML-2 (red) and HL-60 (cyan) fitted with normal distributions. (c) Histograms of AML-2 (red) and HL-60 (cyan) cell diameters fitted with normal distributions. (For interpretation of the references to color in this figure legend, the reader is referred to the web version of this article.)

AML-2 and HL-60. The diameters of the cells were estimated on the basis of the geometrical model with Poisson's ratio of 0.5 (Fig. 6(c)). The cells within the diameter range of 10.5–13 μm were chosen, since the majority of these two types of cells fell in this range ($>70\%$ for AML-2 and >80 for HL-60), and within this range, the cell diameters of these two cell types heavily overlapped. The range of interests was divided into 5 sub-ranges (10.5–11 μm, 11–11.5 μm, 11.5–12 μm, 12–12.5 μm 12.5–13 μm), the average specific membrane capacitance and cytoplasm conductivity values of the cells within each range are shown in SI Fig. S3. For a certain cell type, the specific membrane capacitance and cytoplasm conductivity values of the 5 diameter sub-ranges are all fairly close to the population's average, and the differences of the specific membrane capacitance and cytoplasm conductivity values for AML-2 and HL-60 are almost the same across all the sub-ranges, indicating the different electrical properties of AML-2 and HL-60 measured using our device truly result from the different electrical properties of the cells, rather than the diameter variation.

Specific membrane capacitance and cytoplasm conductivity values are inherent electrical properties of the cells, which should ideally be completely independent of cell size. However, as the cell diameter increases, our measurement results show a very minute increase trend of the specific membrane capacitance and cytoplasm conductivity values for both AML-2 and HL-60 cells. Since this trend of increase is too small to be noticeable in Fig. S3 (a) and (b), the measured specific membrane capacitance and cytoplasm conductivity values of AML-2 and HL-60 within each diameter range are summarized in Table S1. This trend may result from measurement errors caused by the use of the simplified geometrical model. The quasi-spherical cap's surface area is used as the effective area for all the cells to calculate the specific membrane capacitance. Cells with larger diameters may result in slightly larger effective area (vs. cells with smaller diameters) due to the squeeze of the channel, which can cause an increase in the specific capacitance membrane calculation (Eq. (4)). The cytoplasm conductivity estimation assumes a uniform current distribution inside the cell membrane. The different quasi-spherical caps may alter the current distributions inside the cytoplasm, and consequently affect the calculated cytoplasm conductivity value. Overall, the measurement errors caused by cell diameter variation on the determined specific membrane capacitance and cytoplasm conductivity values are small. Thus, the electrical property values are valid for representing the population of a certain cell type. In fact, the results obtained using our technique are consistent with the values reported in electrorotation studies, which are also based on the single shell model (specific membrane capacitance of HL-60: 15 ± 1.9 mF/m^2, 15.6 ± 0.9 mF/m^2; specific membrane capacitance of human granulocytes: 11.0 ± 3.2 mF/m^2; and cytoplasm conductivity of human granulocytes: 0.60 ± 0.13 S/m (Huang et al., 2007; Yang et al., 1999)). Table S2 summarizes comparisons between electrorotation and our technique.

4.5. Cell type classification

Since AML-2 (diameter: 12.5 ± 1.3 μm) and HL-60 (diameter: 11.4 ± 0.93 μm) cells have comparable diameters, the Coulter counter technique produced a low classification success rate of 67.7%. With additional information on cells' electrical properties, these two cell types were better classified. A back propagation neural network was used for pattern recognition. The input data have 3 parameters (diameter, specific membrane capacitance, and cytoplasm conductivity) measured on each cell. Cell type classification success rates were 67.7% (diameter only), 84.4% (diameter+cytoplasm conductivity), 88.6% (diameter+specific membrane capacitance), and 93.0% (diameter+cytoplasm

conductivity+specific membrane capacitance), suggesting that using specific membrane capacitance and cytoplasm conductivity can significantly improve the classification success rate (vs. only using cell diameter/size as in Coulter counter; see Fig. S4). This result is not surprising, as shown in Fig. S3, for the two cell types within the same diameter range, their inherent electrical properties (specific membrane capacitance: P value $< 10^{-150}$, cytoplasm conductivity: P value $< 10^{-70}$) are significantly different. These inherent electrical properties contain additional information (cell membrane and cytoplasm properties) to cell size.

5. Conclusion

This paper demonstrated a new technology for rapid characterization of single-cell electrical properties (specific membrane capacitance and cytoplasm conductivity). The cells are aspirated through a constriction channel, and impedance profiles at 7 different frequencies are measured simultaneously. Geometrical and electrical models were developed to quantify the specific membrane capacitance and cytoplasm conductivity from the experimental impedance data. Compared with previously reported techniques for single-cell electrical characterization, the speed of our system is significantly higher (5–10 cells/s vs. minutes/cell). A total of 3249 AML-2 cells and 3398 HL-60 cells were tested, and the specific membrane capacitance values were determined to be 12.0 ± 1.44 mF/m^2 and 14.5 ± 1.75 mF/m^2, respectively, while cytoplasm conductivity values were determined to be 0.62 ± 0.10 S/m and 0.76 ± 0.12 S/m. The measurements can be used for cell type classification or provide additional information on cells' physiological conditions.

Acknowledgments

Financial support from the Natural Sciences and Engineering Research Council of Canada (NSERC) through a Strategic Grant, from the University of Toronto through a Connaught Innovation Award, and from the Canada Research Chairs Program is acknowledged.

Appendix A. Supporting information

Supplementary data associated with this article can be found in the online version at http://dx.doi.org/10.1016/j.bios.2012.10.081.

References

Bathe, M., Shirai, A., Doerschuk, C.M., Kamm, R.D., 2002. Biophysical Journal 83 (4), 1917–1933.
Chen, J., Zheng, Y., Tan, Q., Zhang, Y.L., Li, J., Geddie, W.R., Jewett, M.A.S., Sun, Y., 2011a. Biomicrofluidics 5 (1), 014113.
Chen, J., Zheng, Y., Tan, Q.Y., Shojaei-Baghini, E., Zhang, Y.L., Li, J., Prasad, P., You, L.D., Wu, X.Y., Sun, Y., 2011b. Lab on a Chip 11 (18), 3174–3181.
Cho, S.B., Thielecke, H., 2007. Biosensors and Bioelectronics 22 (8), 1764–1768.
Cristofanilli, M., De Gasperis, G., Zhang, L.S., Hung, M.C., Gascoyne, P.R.C., Hortobagyi, G.N., 2002. Clinical Cancer Research 8 (2), 615–619.
De Gasperis, G., Wang, X.B., Yang, J., Becker, F.F., Gascoyne, P.R.C., 1998. Measurement Science and Technology 9 (3), 518–529.
Duncan, L., Shelmerdine, H., Hughes, M.P., Coley, H.M., Hubner, Y., Labeed, F.H., 2008. Physics in Medicine and Biology 53 (2), N1–N7.
Gamliel, H., Gurfel, D., Polliack, A., 1983. Journal of Clinical Immunology 3 (4), 399–407.
Geng, T., Zhan, Y.H., Wang, J., Lu, C., 2011. Nature Protocols 6 (8), 1192–1208.
Gifford, S.C., Frank, M.G., Derganc, J., Gabel, C., Austin, R.H., Yoshida, T., Bitensky, M.W., 2003. Biophysical Journal 84 (1), 623–633.
Han, K.H., Han, A., Frazier, A.B., 2006. Biosensors and Bioelectronics 21 (10), 1907–1914.
Hochmuth, R.M., 2000. Journal of Biomechanics 33 (1), 15–22.
Hoffman, R.A., Britt, W.B., 1979. Journal of Histochemistry and Cytochemistry 27 (1), 234–240.
Holzel, R., 1999. BBA Molecular Cell Research 1450 (1), 53–60.
Huang, C.J., Chen, A.L., Wang, L., Guo, M., Yu, J., 2007. Biomedical Microdevices 9 (3), 335–343.
Huang, Y., Wang, X.B., Holzel, R., Becker, F.F., Gascoyne, P.R.C., 1995. Physics in Medicine and Biology 40 (11), 1789–1806.
Lam, W.A., Rosenbluth, M.J., Fletcher, D.A., 2007. Blood 109 (8), 3505–3508.
Li, S., Lin, L.W., 2007. Sensors Actuators A—Physical 134 (1), 20–26.
Rodriguez, Carlos M., Barbara Carrillo, J.M.C., Gordon, Kristie M., Horton, Allan F., Paul, Ronald D., Wells, Mark A., Wyatt, James L., 2001. Method and apparatus for analyzing cells in a whole blood sample, Patent no. US6228652.
Rosenbluth, M.J., Lam, W.A., Fletcher, D.A., 2008. Lab on a Chip 8 (7), 1062–1070.
Sequeira, Melwyn F., Goltman, M.M.-K. Isay, 2001. DC/RF blood cell detector using isolated bridge circuit having automatic amplitude and phase balance components, Patent no. 6204668.
Schwake, L., Henkel, A.W., Riedel, H.D., Stremmel, W., 2002. Blood Cells, Molecules and Diseases 29 (3), 459–464.
Schwan, H.P., 1957. Advances in Biological and Medical Physics 5, 147–209.
Schwan, H.P., 1968. Annals of the New York Academy of Sciences 148 (1), 191–209.
Sun, T., Morgan, H., 2010. Microfluidics and Nanofluidics 8 (4), 423–443.
Valero, A., Braschler, T., Renaud, P., 2010. Lab on a Chip 10 (17), 2216–2225.
Wang, H.Y., Lu, C., 2006. Analytical Chemistry 78 (14), 5158–5164.
Wang, X.B., Huang, Y., Gascoyne, P.R.C., Becker, F.F., Holzel, R., Pethig, R., 1994. BBA-Biomembranes 1193 (2), 330–344.
Yang, J., Huang, Y., Wang, X.J., Wang, X.B., Becker, F.F., Gascoyne, P.R.C., 1999. Biophysical Journal 76 (6), 3307–3314.
Yap, B., Kamm, R.D., 2007. Journal of Applied Physiology 102 (4), 1729–1731.
Zhao, Y., Inayat, S., Dikin, D.A., Singer, J.H., Ruoff, R.S., Troy, J.B., 2008. Proceedings of the Institution of Mechanical Engineers, Part N: Journal of Nanoengineering and Nanosystems 222 (1), 1–11.
Zheng, Y., Shojaei-Baghini, E., Azad, A., Wang, C., Sun, Y., 2012. Lab on a Chip 12 (14), 2560–2567.
Zimmermann, D., Zhou, A., Kiesel, M., Feldbauer, K., Terpitz, U., Haase, W., Schneider-Hohendorf, T., Bamberg, E., Sukhorukov, V.L., 2008. Biochemical and Biophysical Research Communications 369 (4), 1022–1026.
van Berkel, C., Gwyer, J.D., Deane, S., Green, N., Holloway, J., Hollis, V., Morgan, H., 2011. Lab on a Chip 11 (7), 1249–1255.